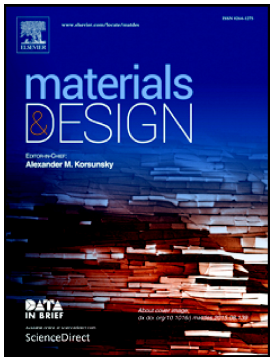

Compositional design of Fe-based multi-component bulk metallic glass based on CALPHAD method

J.J. Han, C.P. Wang, J. Wang, X.J. Liu, Y. Wang, Z.K. Liu

PII: S0264-1275(17)30386-6
DOI: doi: 10.1016/j.matdes.2017.04.030
Reference: JMADE 2952

To appear in: *Materials & Design*

Received date: 15 December 2016
Revised date: 8 April 2017
Accepted date: 10 April 2017

Please cite this article as: J.J. Han, C.P. Wang, J. Wang, X.J. Liu, Y. Wang, Z.K. Liu , Compositional design of Fe-based multi-component bulk metallic glass based on CALPHAD method. The address for the corresponding author was captured as affiliation for all authors. Please check if appropriate. Jmade(2017), doi: 10.1016/j.matdes.2017.04.030

Compositional design of Fe-based multi-component bulk metallic glass based on CALPHAD method

J. J. Han,[a] C. P. Wang,[a] J. Wang,[b] X. J. Liu,[a,,] Y. Wang,[c] Z. K. Liu[c]*

[a] College of Materials and Fujian Key Laboratory of Materials Genome, Xiamen University, Xiamen 361005, P. R. China

[b] Department of Materials Physics, School of Physics and Optoelectronic Engineering, Nanjing University of Information Science & Technology, Nanjing 210044, P. R. China

[c] Department of Materials Science and Engineering, Pennsylvania State University, University Park, Pennsylvania 16802, U. S. A.

A quantificational composition design protocol (CDP) of Fe-based bulk metallic glasses (BMGs) with excellent glass-forming ability (GFA) has been proposed on the basis of the thermodynamic calculations. The stability of liquid and the crystallization of solids were both evaluated from the perspective of atomic structure and local composition. The present protocol successfully associates the stability of liquid to the melting point of alloy and the difficulty of crystallization by considering the type and competition of potential equilibrated phases. Specifically, this protocol provided the selection criteria of phases and elements from the viewpoint of structure and composition fluctuations during nucleation for each phase, whose accuracy and effectiveness were experimentally verified.

Keywords: bulk metallic glasses; composition design protocol; potential crystalline phases; phase diagram

1. Introduction

Fe-based bulk glassy alloys have recently gained popularity due to their excellent soft magnetic properties, high electrical resistivity, high mechanical strength and good economic benefit, compared to other glassy alloys [1-4]. Since the first Fe-based bulk metallic glass (BMG) was fabricated in 1995 [5], a huge number of Fe-based multi-component glassy alloys in metal-metalloid systems have been successfully developed [6-9]. The relatively low cost and excellent performance result the Fe-based metallic glasses to be one of the most technologically important class of alloys. However, Fe-based metallic glasses are highly complex alloys, since they often involve 3 or more solute elements and a large concentration of metalloid and non-metal elements. Consequently, accurate prediction of glass-forming ability (GFA) and compositional design for Fe-based multi-components alloys remains a prevalent challenge.

In the past few decades, several empirical rules have been introduced to estimate the GFA of various multi-component alloys [10-13]. Metallic glasses can be formed by solidification of liquid alloys at sufficiently high cooling rates to suppress the nucleation and growth of competing crystalline phases. The preservation of a supercooled liquid structure depends substantially on two factors: the stability of the supercooled liquid, and the difficulty of crystallization. The characteristics of metallic liquid have been extensively studied that the composition of alloy with good GFA is roughly located at the composition of eutectic point [11, 14-20], where the liquid is relatively stable against others through optimal dense structural topology [21-23]. However, this criterion does not always work in practice, and the difficulty in actual implement increases along the increasing number of alloying elements. Using this method to exactly determine the excellent glass-forming compositions especially for Fe-based system remains challenge [2, 24, 25]. Up to now, no systematic and comprehensive manner protocol of quantifiable evaluation on the GFA of Fe-based multi-component alloys is available. A scientific approach rather than trial-and-error method to search the compositions of formation materials of Fe-based multi-component

glass is imperative.

Recently, the calculation of phase diagram (CALPHAD) method derived from the experimental data of thermodynamic properties and phase equilibria has been successfully applied in the design of materials with specific technological properties [26-28]. In addition, CALPHAD can be employed to calculate the driving forces of crystalline phases in a supercooled liquid. The GFA and glass-forming range of an alloy system can be predicted by driving force criterion with the obtained thermodynamic description for the investigated system [29-31]. However, little work has been done to quantitatively predict the glass-forming composition for multi-component alloys.

It is well known that crystallization usually starts with nucleation. Therefore, the high GFA can be sophisticatedly predicted by searching a condition when the nucleation of crystalline phases can be retarded to some extent. The condition in the present work covers the difference of composition and structure between supercooled liquid and potential crystalline phases. In this scenario, the present work tends to clarify the main potential crystalline phases from supercooled liquid characterized by their structures and compositions, and more importantly, reveal the influence of these phases on the GFA of alloys. Based on present results, a composition design protocol (CDP) for Fe-based multi-component BMGs will be proposed, by which one can readily select the appropriate alloying elements and their contents that facilitate the formation of glass. The practicality and efficiency of this protocol would be validated by the previous and present experiments.

2. Methodology and procedure

2.1. Alloy design strategy

The CALPHAD approach has been used to describe the thermodynamic properties of solid solutions and compounds as a function of temperature [32], which was defined relative to the stable element reference, meaning enthalpies of the pure elements in their defined reference phase at 298.15 K and 1 atm. All thermodynamic calculations for the

Fe-based multi-component systems were performed using the Thermo-Calc package [33] in conjunction with the Fe-Data thermodynamic database based on relevant steel subsystems from the SGTE solution database [34, 35]. This data contained in this database includes the elements studied in this work. These calculations attempt to describe the metastable phase formation during the supercooling process in the form of the equilibrium phase diagram.

Reducing the melting point of an alloy is one of the most critical factors for enhancing the GFA [36-38]. Fe-based binary phase diagrams [39] show that carbon (C) and boron (B) are the primary elements to reduce the melting points of the alloys. In addition, enough additions of C or B would robustly suppress the formation of topologically close-packed (TCP) phases, which consists mainly of the metallic bond. TCP with non-directional and unsaturated in nature results in a high coordination number (CN) close to that of the clusters in a supercooled liquid. These features make them easily nucleate from the liquid metal [40-44]. Actually, the current findings of dominant Fe-based BMGs are all metal-metalloid system, of which the GFA is highly associated with the metalloid elements [45].

In light of the critical role of C and B on the formation of Fe-based BMGs, Fe-C and Fe-B pseudo-binary phase diagrams were constructed for the high-order systems. In these diagrams, the phase boundaries resulted from the variation of more than two of the element contents are calculated by fixing the concentrations of C or B elements. The alloying elements considered in the present work include Cr, Mn, Mo, Co, Ni, Cu, V, W, Nb, Ti, Zr, B, C, Al, Si, and Y. The calculated mass fraction of phase is employed to estimate the nucleation rate for each potential phase.

2.2. Experimental procedure

All multi-component alloy ingots were prepared by arc-melting a mixture of pure (>99 at.%) Fe, Cr, Mo, C, B and Y under a Ti-gettered pure argon atmosphere. The ingots were remelted at least four times to ensure the homogeneity of the multicomponent alloys. Cylindrical rods with a diameter of 3mm were then fabricated by a water-cooled

copper mold method under argon atmosphere. Phase identification in the as-cast samples was examined by X-ray diffraction (XRD) with Cu *Kα*radiation. The morphology was determined by electron probe microanalysis (EPMA).

3. Determination of a favorable phase

3.1. Phases in Fe-based alloy

Although a large number of phases with distinct constituent and structure would potentially form in the Fe-based alloys, quite enumerable types of phases are actually found near the eutectic point in Fe-C based and Fe-B based systems [34, 35]. The formula units about the relevant phases are listed in Table 1. It is noted that the TCP phases are absent in the presence of metalloid elements by which the melting point of Fe-based alloys is remarkably reduced. Generally, these potential crystalline phases can be classified into solid solution and compound. It is fortunate that this classification is also in accord with the role of phases on the GFA of alloy, which will be discussed in the following sections.

3.2. Selection principle of phases

In general, GFA is determined by both the thermodynamic and kinetic parameters [46], which have been proven to be especially pronounced for multi-component systems [2]. For a multi-component metal liquid, the early stage of crystallization frequently requires a change in local composition, and a long-range diffusion is needed to establish the difference in composition between the liquid and the growing crystalline phase. This type of diffusion is a long timescale process, which would slow down crystalline nucleation and facilitate glass formation. Therefore, an excellent GFA can be obtained when the local atomic structure and composition in supercooled liquid are dramatically different from those of crystalline phases potentially precipitated upon cooling [47]. On the other hand, the equilibrium phases near liquidus temperature should exhibit compositional competition. The more the phases tend to precipitate, the better the competitive effect is.

The solid solutions incorporated with substitutional or interstitial solute have more closed-packed structures than the TCP phases, featured by non-directional and unsaturated metallic bonds. Their high CNs close to the atomic clusters in a supercooled liquid and low energy barriers for phase transition both make atoms easily rearrange during crystallization [48-50]. In addition, the solid solution generally has a wide composition range [41, 43] and disorder crystal structure, allowing direct nucleation without drastic composition fluctuation. In consideration of the above two items, suppressing the formation of solution phase is primary to obtain the glassy structure from supercooled liquid. The thermodynamic database indicates that there are four types of solid solutions in the Fe-based alloys (as shown in Table 1), namely face centered cubic (FCC) solid solution (austenite), body centered cubic (BCC) solid solution (α-ferrite), hexagonal close packed (HCP) phase (non-stoichiometric Co-, Ti-, Zr-rich M_2C carbide), and MC (non-stoichiometric V-, Ti-, Nb-, Zr-rich fcc MC carbide). Unfortunately, our calculations of the phase equilibrium demonstrate that it is scarcely possible to suppress these solid solutions owing to the metallic nature of Fe-based alloy. However, suppressing the easy-forming solid solution phase is practicable. Here, the term "easy-forming" refers to the probability of nucleation driven by transition pathway from amorphous structure in the supercooled liquid to crystalline structure [51]. The atomic structure for solid solution phases is so simple that the rearrangement rate of small metalloid atoms during the process of nucleation is more comparable to solvent atoms than that of compounds with complex structure. The solubility of both B and C in austenite is much greater than those in ferrite, even if other alloying elements substituting Fe change the pristine lattice constant [52, 53]. To this end, ferrite requires much more drastic composition fluctuation to nucleate from supercooled liquid than austenite, leading to a longer incubation period. In the thermodynamic model, the MC carbide, where the number of C atoms siting the second sub-lattice is more than those in both ferrite and austenite, is treated as an FCC solid solution. Evidently, our calculations of phase equilibria found the frequent existence of the two-phase region of FCC solid solution and MC carbide, suggesting that the FCC matrix can facilitate the precipitation of MC phase. Differing from other solid solution phases, the HCP phase is an Fe-depleted carbide with much higher content of C. Also,

the contents of Fe and C for HCP phase are comparable with some typical complex carbides, such as $M_{23}C_6$ and M_7C_3, which means if the HCP phase serves as the equilibrated phase with $M_{23}C_6$ and M_7C_3 carbides, the nucleation would be dramatically retarded. More recently, the present authors have examined the transitions from the cluster in the supercooled liquid state to the crystalline cluster at the atomic level [51]. It is found that the FCC atomic clusters have more stable and metastable configurations than BCC or HCP atomic clusters, as shown in Fig. 1. In this scenario, the FCC phase, regardless of the atomic structure in the supercooled liquid state, has a higher probability of nucleation compared to BCC or HCP from the viewpoint of transition pathway. Moreover, another work reveals that the stability of these clusters in each size is only weakly dependent on their compositions [54]. In consideration of suppressing the easy-forming solid solution phase, FCC solid solution and MC carbide are highly unacceptable, whereas HCP solid solution is allowed to exist equilibrating with adequate competitive phases, and the BCC solid solution phase comes second.

Due to the presence of large amount of C and/or B, the covalent bond in Fe-based alloy becomes prominent, resulting in the formation of various compounds, namely cementite, Ksi-carbide, Shp-MC, M_3C_2, $M_{23}C_6$, M_6C, M_7C_3 and M_aB_c (a and c are stoichiometric factors). These compounds are of nearly-stoichiometric with respect to C and/or B, except for Shp-MC, which can be treated as a simple HCP solid solution. Similar to solid solutions, the nucleation of compound phases is also controlled by the process of composition and structure fluctuations. In Fe-based alloy melt near the eutectic point, the atomic structures with central solute atoms of B and C are close packing in the first shell, with CNs greater than 8 [19]. While in the carbides, the CN of the solute atom at each site is somewhat reduced, *e.g.*, 8 for cementite, (7, 8) for M_3C_2, 8 for $M_{23}C_6$, 6 for M_6C, and (5, 5, 9) for M_7C_3. This means that the onset of nucleation especially for M_6C and M_7C_3 compounds would be retarded by remarkable composition fluctuation upon cooling. For borides, the transition metal elements occupying at M sites generally have strict stoichiometric ratio and ordered configuration, in contrast to the disordered configuration in the supercooled liquid. On the other hand, the atomic structure of Fe-based supercooled liquid, similar to Fe-based metallic glasses, is

constructed by unique distorted trigonal prisms and anti-Archimedean prisms with B central atoms [55]. From the dispersive distribution of B atoms in the supercooled liquid state to their attractive nature of bonding in borides, the resulting long-range atomic rearrangement of the constituent atoms has positive effects on reducing nucleation rate. The effects of each phase on the GFA of Fe-based alloys have been summarized in Table 1, where the positive effect and negative effect are denoted by corresponding symbols.

3.3. Compositional competition amongst phases

As discussed above, a good GFA could be obtained when the atomic structure, and more significantly, the local composition of the supercooled liquid are dramatically different from those of the potential precipitates during cooling [47]. Besides taking account of the feature for each phase, for a multi-component metal system, the compositional competition caused by equilibrium phases also play a crucial role on the glass formation of supercooled liquid. Thus, an Fe-Based alloy with excellent GFA must meet the following requirements: 1) composition of potential precipitated phases largely deviates from that of the liquid; 2) potential equilibrium phases at temperatures approaching the solidus curve are competitive with each other in terms of composition. To demonstrate the correlation between GFA and compositional competition, the calculated fractions of selected components in each phase as a function of temperature were employed. In this work, four typical Fe-based multicomponent alloys, i.e., $Fe_{65}Cr_{14}C_{15}B_6$, $Fe_{50}Mo_{14}Cr_{15}C_{15}B_6$, $Fe_{57}Mo_{10}Cr_{12}C_{15}B_4Y_2$ and $Fe_{48}Mo_{14}Cr_{15}C_{15}B_6Y_2$, were considered (see Fig. 2). The compositions of the alloys are arranged by their order in the GFA: $Fe_{65}Cr_{14}C_{15}B_6$ < $Fe_{50}Mo_{14}Cr_{15}C_{15}B_6$ ≈ $Fe_{57}Mo_{10}Cr_{12}C_{15}B_4Y_2$ < $Fe_{48}Mo_{14}Cr_{15}C_{15}B_6Y_2$ [2, 56]. Corresponding to Table 1, the red curves in Fig. 2 denote phases which are positive for glass formation and the green curves denote those negative. Particularly, the blue curve represents $M_{23}C_6$ compound, of which the effect on GFA depends on the matrix phase. From Fig. 2(a), Fig. 2(b) and Fig. 2(i), the main potential crystalline phases for $Fe_{65}Cr_{14}C_{15}B_6$ alloy include FCC, Fe_2B, cementite, and M_7C_3 when the liquid is cooled into supercooled state. As the temperature decreases,

M_7C_3 compound and FCC solid solution primarily appears in the supercooled liquid, serving as equilibrium phases in a large temperature region. It is clear that the composition of FCC solid solution is Fe-rich, Cr-depleted, and C-depleted, whereas M_7C_3 compound has composition of Fe-depleted, Cr-rich, and C-rich, just in contrast to FCC solid solution. This implies the nucleation of the M_7C_3 compound would be facilitated by the compositional fluctuation from the formation of FCC solid solution. The lack of compositional competition between M_7C_3 compound and FCC solid solution has a negative effect on the glass formation, although the former is an individually reliable phase to retard nucleation. In a deeper supercooled liquid region, cementite starts to nucleate in a ready manner, owing to its steady fractions of components as supercooled liquid. Actually, the primary phases have largely determined the GFA of supercooled liquid. For cementite the negative effect on GFA is far less than the primary phases (M_7C_3 compound and FCC solid solution) due to the sluggish motion of atoms at lower temperature. Anyway, $Fe_{65}Cr_{14}C_{15}B_6$ alloy is definitely a poor glass former account for the primary FCC solid solution and weak compositional competition between phases. Situation is dramatically changed after 14 at.% Mo is added into the pristine alloy, as shown in Fig. 2(c), Fig. 2(d) and Fig. 2(j). The appearance of many new types of phases can be observed such as HCP, an Fe-depleted, Cr-depleted and C-rich phase; M_6C, an Fe-depleted phase; Ksi-carbide, an Fe-depleted, Cr-depleted and C-rich phase; $M_{23}C_6$, a Cr-rich and C-rich phase. In the presence of these phases, each component in liquid hardly meets the nucleation conditions for all crystalline phases simultaneously. As a result, these equilibrium phases become much more competitive. Here, one highlighted positive change that benefits the GFA is the partial substitution of FCC solid solution by Fe-depleted HCP phase, which is competitive with Fe-depleted and C-rich compounds other than its individual positive effect on the GFA. Although FCC solid solution can still be observed in a large temperature region, the GFA of alloy has been significantly improved. For the $Fe_{57}Mo_{10}Cr_{12}C_{15}B_4Y_2$ alloy (see Fig. 2(e), Fig. 2(f) and Fig. 2(k)), the amounts of Mo and Cr are reduced and additionally 2 at.% Y is added. Fe-depleted M_6C compound vanishes, and instead BCC solid solution partially substitutes FCC solid solution. Thus, the former deteriorates the GFA, while the latter benefits it. These two

aspects somewhat balance each other out in the present case, resulting in a moderate change in GFA. In the final $Fe_{48}Mo_{14}Cr_{15}C_{15}B_6Y_2$ alloy (see Fig. 2(g), Fig. 2(h) and Fig. 2(l)), the addition of Y substitutes Fe rather than Mo and Cr. Results show that Fe-depleted M_6C compound, the same as the $Fe_{57}Mo_{10}Cr_{12}C_{15}B_4Y_2$ alloy, also vanishes completely. However, the FCC solid solution loses original stability in a large temperature region, overwhelmed by BCC and HCP solid solutions. According to our discussion before, BCC solid solution has a low nucleation rate from viewpoint of transition pathway, compared with FCC solid solution; HCP solid solution is an Fe-depleted and C-rich phase, which makes it become a promising competitive phase with complex compounds, such as M_6C, M_7C_3 and $M_{23}C_6$. It is evident that the inhibition of FCC solid solution phase is the most crucial approach for improving the GFA of multi-component Fe-based alloy.

Concerning compositional fluctuation, $M_{23}C_6$ is less effective on GFA than M_7C_3, M_6C and Ksi-carbide, because smaller compositional fluctuation is needed for the nucleation of $M_{23}C_6$ compound. From Fig. 2, if $M_{23}C_6$ compound serves as the equilibrium phase with other carbides, the process of primary crystallization is supposed to be retarded due to the competition of Cr-rich and C-rich properties. However, experimental study found that the $M_{23}C_6$ compound with a complex FCC structure frequently precipitates on the grain boundary of austenite in steel [57]. This means that the nucleation of $M_{23}C_6$ compound could be facilitated in the presence of austenite matrix. Thus, if so for the case upon rapid cooling, $M_{23}C_6$ compound would not be qualified for the competitive phase when FCC solid solution exists. To verify this hypothesis, studies on the correlation between calculated phase equilibria in terms of $M_{23}C_6$ compound and actual precipitations upon rapid cooling were carried out in the present work. Table 2 lists the alloy compositions for experiment as well as the reactions upon cooling calculated from phase diagram. Here, the $M_{23}C_6$ phase at low temperatures is not presented. It is experimentally found that the $M_{23}C_6$ phase is precipitated upon rapid cooling without exception in the alloys with primary phase of FCC solid solution (austenite) (see Fig. 3). However, the state of $M_{23}C_6$ phase in these cases should be metastable, whose compositions deviate from the stable one as described in the phase diagram.

Distinguishingly, $M_{23}C_6$ phase could not be identified by XRD patterns in the $Fe_{52}Cr_{10}Mo_{12}C_{16}B_8Y_2$ alloy. From Table 2, the FCC solid solution retreats from the primary phases for $Fe_{52}Cr_{10}Mo_{12}C_{16}B_8Y_2$ alloy in a high temperature region. Instead, HCP solid solution and MoB compound serve as the potential primary phases. By systematically finalizing present results, it is clear that the formation of $M_{23}C_6$ phase can be facilitated by FCC solid solution matrix rather than BCC or HCP solid solutions. That means the Cr-rich $M_{23}C_6$ compound is allowed to exist only without the FCC matrix, although it has lower priority compared to M_6C and M_7C_3 compounds. In comparison with carbides, most of the borides, except for Fe_2B and M_2B, are Fe-depleted and B-rich compounds with B-B bonds in the first neighbor shell. Thus, it is expected that there are as many as possible borides serving as potential phases, competing with each other in terms of composition.

Now that it has been clarified which phases are positive for the GFA of Fe-based liquid alloy and how the couples of these phases yield the greatest obstacle to the nucleation of primary phases.

3.4. Selection principle of elements

After figuring out the selection principle of phases, it is consequently needed a guideline on the selection of elements. In the present work, the effects of a single element on the stability of various phases were firstly clarified, and then rough assessments were carried out by considering the comprehensive effects. On the basis of calculations using thermodynamic database the performances of essential elements, including Cr, Mn, Mo, Co, Ni, Cu, V, W, Nb, Ti, Zr, B, C, Al, Si, and Y, on each phase were illustrated, treated as three levels, namely positive, moderate and negative. According to the information summarized in Table 3, ones can readily pick up the compatible elements to take positive role in the formation of the desirable phases without conflict. For example, the element of W, from Table 3, exhibits a positive effect on the formation of ferrite, borides, and MC carbide. It has been clarified that the former two phases are individually beneficial to the GFA of Fe-based alloy, whereas the last one would deteriorate GFA in the presence of C element. Therefore, the basic system

with reference to W is Fe-W-B rather than Fe-W-C. Bearing in mind the principle of suppressing the easy-forming solid solution phase and compositional competition, the elements of Co, Cr, Mo, V, Nb, Ti, Zr, Si and Al, on the one hand, are candidates since they are HCP and BCC solid solutions formers; the elements of Ni, Mn, Cr, Mo, V, Nb, Ti and Zr, on the other hand, are potential additives since they are M_aB_b and MB_2 formers. However, special attention should be paid to the elements of Ni and Mn which are typical austenite formers, and also none of Co, Si and Al elements is boride formers. The final optimized system without C addition is hence determined to be Fe-(Co, Si, Al)-Cr-Mo-V-W-Nb-Ti-Zr-B, where the elements bracketed together should be low addition. It is noteworthy that Ni, Mn, Cu elements are banned in this system. Considering the existence of element C, V, W, Nb, Ti, Zr are not allowed to add any more because they are all strong MC formers. In contrast, Mo and Cr are the necessary elements which are the primary candidates to induce the formation of complex carbides, such as $M_{23}C_6$, M_6C and M_7C_3. Promisingly, both of Mo and Cr are HCP and BCC solid solutions formers so that the FCC austenite would lose stability. Hence, the final system with C addition would be roughly based on Fe-(Co, Si, Al)-Cr-Mo-C. In view of the ability of alloy elements in the formation of M_aB_b and MB_2 borides, a derived system of Fe-(Co, Si, Al)-Cr-Mo-C-B can be obtained. Another important category of additives are rare earth elements (Re), the role of which has been attributed to refine the constituent of alloy by absorbing oxygen [58, 59]. However, the findings from our calculations indicate that the small addition of rare earth elements, Y for example, has in addition a significant effect on suppressing the primary formation of solid solutions. The excessive addition of Re would nevertheless take a negative effect on the GFA of Fe-based alloy. It is suggested the limited amount of Re additives to avoid the consumption of B and C by the formation of rare earth carbide and boride.

In the framework of the proposed Fe-(Co, Si, Al)-Cr-Mo-V-W-Nb-Ti-Zr-B-RE, and Fe-(Co, Si, Al)-Cr-Mo-C-B-RE alloy systems, the phase diagram can then be calculated by introducing thermodynamic database. The GFA of alloys quantitatively depends on the phase relations and phase fractions. In Fig. 4, we plotted the flow diagram of composition design protocol for Fe-based BMGs.

4. Design of BMGs and experimental verification

Before experiments were carried out, the well-developed alloy systems were firstly introduced to validate the CDP for Fe-based BMGs. Table 4 lists the current typical BMG systems from literatures [2]. It can be seen that the components of these BMG systems, without exception, basically follow the selection principle of elements proposed by this work. Here, the specific compositions have not been verified, in consideration of the current incomplete database. Even so, the composition sensitivity of BMGs is fundamentally in consistence with the intricate phase relation of multi-component systems, which illustrates that the GFA of BMGs, especially for multi-component systems, is largely controlled by competitive phases.

To quantitatively examine the accuracy of the CDP, some independent systems and compositions were considered to establish the corresponding relation between theoretical prediction and experimental results. In the present paper, a comparison experiment schemed by two different compositions in Fe-Cr-Mo-C-B-Y system were shown as an example. Figure 5 shows the calculated isopleth section in terms of the equilibrium phases of $Fe_{63-x}Cr_{16}Mo_{13}B_6Y_2C_x$ multi-component system. The grey area denotes the composition region of easy glass-forming according to the criteria of phase selection. In this system, two compositions, namely $Fe_{53}Cr_{16}Mo_{13}B_6Y_2C_{10}$ and $Fe_{50}Cr_{16}Mo_{13}B_6Y_2C_{13}$, respectively inside and outside the grey area were chosen as a comparison experiment. Then, the weight fractions of phases as a function of temperature for $Fe_{53}Cr_{16}Mo_{13}B_6Y_2C_{10}$ and $Fe_{50}Cr_{16}Mo_{13}B_6Y_2C_{13}$ alloys were calculated, as shown in Fig. 6. It can be seen that the potential precipitates for these two compositions mostly meet the criteria of phase selection. However, there are significant fractions of FCC and MC phases in the temperature region of 1200-1300 K for both alloys. By comparison, $Fe_{53}Cr_{16}Mo_{13}B_6Y_2C_{10}$ alloy has a smaller fraction and temperature region of FCC phase, a larger fraction of BCC phase, and a lower melting point than $Fe_{50}Cr_{16}Mo_{13}B_6Y_2C_{13}$ alloy. Accordingly, the GFA of $Fe_{53}Cr_{16}Mo_{13}B_6Y_2C_{10}$ alloy should be stronger than that of $Fe_{50}Cr_{16}Mo_{13}B_6Y_2C_{13}$ alloy. Then, the experiments were carried out to verify the predictive validity. Figure 7 shows the XRD patterns and

EPMA of as-cast $Fe_{53}Cr_{16}Mo_{13}B_6Y_2C_{10}$ and $Fe_{50}Cr_{16}Mo_{13}B_6Y_2C_{13}$ rods with a diameter of 3 mm. The results from XRD patterns as well as EPMA indicate that the as-cast $Fe_{53}Cr_{16}Mo_{13}B_6Y_2C_{10}$ alloy has a full amorphous structure characterized by diffuse maximum and uniform morphology, whereas the as-cast $Fe_{50}Cr_{16}Mo_{13}B_6Y_2C_{13}$ alloy has a mixed structure of amorphous and crystalline since some distinct diffraction peaks and precipitates can be detected. The consistency of theoretical perdition and experimental results prove the accuracy of the proposed CDP of Fe-based BMGs.

5. Conclusion

In this work, an accurate and effective composition design protocol for Fe-based bulk metallic glass was proposed. Different from the previous methods that associate the glass-forming ability of alloy with the melting point and the drive force of crystalline phases, this protocol emphasizes the process of nucleation in terms of compositional and structural fluctuations. From the perspective of atomic structure and local composition, the effects, i.e., positive or negative, of each phase on the GFA of Fe-based alloy were clarified. More significantly, how the couples of these phases yield the greatest obstacle to the nucleation of primary phases was illustrated, based on the concept of component competition. By taking advantage of thermodynamic database, the influences of various alloy elements, including Cr, Mn, Mo, Co, Ni, Cu, V, W, Nb, Ti, Zr, B, C, Al, Si, and Y, on the formation of each phase were listed to provide a guidance for the selection of elements. Finally, the typical Fe-based BMG systems and the designed experiment were introduced to validates the presented composition design protocol. The consistency of theoretical perdition and experimental results prove that this protocol is highly accurate and effective.

Acknowledgements

This work was supported by National Natural Science Foundation of China (Nos. 51601160, 51601096), the Natural Science Foundation of Fujian Province (No.

2016J05133), the Fundamental Research Funds for the Central Universities (No. 20720150079), the Natural Science Foundation of Jiangsu Province (No. BK20160958).

References

[1] A. Inoue, B.L. Shen, A New Fe-based Bulk Glassy Alloy with Outstanding Mechanical Properties, Adv. Mater. 16 (2004) 2189-2192.

[2] C. Suryanarayana, A. Inoue, Iron-based bulk metallic glasses, Int. Mater. Rev. 58 (2013) 131-166.

[3] A. Inoue, Bulk Glassy Alloys: Historical Development and Current Research, Eng. 1 (2015) 185-191.

[4] P. Ramasamy, A. Szabo, S. Borzel, J. Eckert, M. Stoica, A. Bárdos, High pressure die casting of Fe-based metallic glass, Sci. Rep. 6 (2016) 35258.

[5] A. Inoue, J.S. Gook, FE-BASED FERROMAGNETIC GLASSY ALLOYS WITH WIDE SUPERCOOLED LIQUID REGION, Mater. Trans. JIM 36 (1995) 1180-1183.

[6] A.L. Greer, E. Ma, Bulk metallic glasses: At the cutting edge of metals research, MRS Bull 32 (2007) 611-615.

[7] A. Inoue, A. Takeuchi, Recent development and application products of bulk glassy alloys, Acta Mater. 59 (2011) 2243-2267.

[8] M. Chen, A brief overview of bulk metallic glasses, NPG Asia Mater. 3 (2011) 82-90.

[9] Y. Geng, Y. Wang, Z. Wang, J. Qiang, H. Wang, C. Dong, O. Tegus, Formation and structure-property correlation of new bulk Fe–B–Si–Hf metallic glasses, Mater. Des. 106 (2016) 69-73.

[10] P.J. Desre, Thermodynamics and Glass Forming Ability from the Liquid State, MRS Online Proceedings Library Archive 554 (1998) 51 (12 pages).

[11] J. Cheney, K. Vecchio, Prediction of glass-forming compositions using liquidus temperature calculations, Mater. Sci. Eng. A 471 (2007) 135-143.

[12] A.-h. Cai, G.-x. Sun, Y. Pan, Evaluation of the parameters related to glass-forming ability of bulk metallic glasses, Mater. Des. 27 (2006) 479-488.

[13] B. Ramakrishna Rao, M. Srinivas, A.K. Shah, A.S. Gandhi, B.S. Murty, A new thermodynamic parameter to predict glass forming ability in iron based multi-component systems containing zirconium, Intermetallics 35 (2013) 73-81.

[14] P.J. Desre, Thermodynamics and glass forming ability from the liquid state, Mater.

Res. Soc. Symp. Proc. 554 (1999) 51-62.

[15] J.D. Eshelby, Distortion of a Crystal by Point Imperfections, J. Appl. Phys. 25 (1954) 255-261.

[16] T. Fukunaga, H. Sugiura, N. Takeichi, U. Mizutani, Experimental studies of atomic structure, electronic structure, and the electronic transport mechanism in amorphous Al-Cu-Y and Mg-Cu-Y ternary alloys, Phys. Rev. B 54 (1996) 3200-3210.

[17] M. Marcus, D. Turnbull, Correlation between Glass-Forming Tendency and Liquidus Temperature in Metallic Alloys, Mater. Sci. Eng. 23 (1976) 211-214.

[18] D.B. Miracle, A structural model for metallic glasses, Nat. Mater. 3 (2004) 697-702.

[19] D.B. Miracle, W.S. Sanders, O.N. Senkov, The influence of efficient atomic packing on the constitution of metallic glasses, Philos. Mag. 83 (2003) 2409-2428.

[20] D.B. Miracle, O.N. Senkov, Topological criterion for metallic glass formation, Mater. Sci. Eng. A 347 (2003) 50-58.

[21] E.K. Parks, T.D. Klots, S.J. Riley, Chemical Probes of Metal Cluster Ionization-Potentials, J. Chem. Phys. 92 (1990) 3813-3826.

[22] S. Yang, M.B. Knickelbein, Photoionization Studies of Transition-Metal Clusters - Ionization-Potentials for Fen and Con, J. Chem. Phys. 93 (1990) 1533-1539.

[23] S.Y. Wu, S.H. Wei, G.Q. Guo, J.G. Wang, L. Yang, Structural mechanism of the enhanced glass-forming ability in multicomponent alloys with positive heat of mixing, Sci. Rep. 6 (2016) 38098.

[24] J. Cheney, K. Vecchio, Prediction of glass-forming compositions using liquidus temperature calculations, Mater. Sci. Eng. A 471 (2007) 135-143.

[25] A.-h. Cai, H. Wang, X.-s. Li, H. Chen, W.-k. An, Progress of component design methods for bulk metallic glass, Mater. Des. 28 (2007) 2694-2697.

[26] L. Kaufman, Computational thermodynamics and materials design, Calphad 25 (2001) 141-161.

[27] U.R. Kattner, THE CALPHAD METHOD AND ITS ROLE IN MATERIAL AND PROCESS DEVELOPMENT, Tecnol. Metal. Mater. Min. 13 (2016) 3-15.

[28] P.E.A. Turchi, A. Gonis, R.D. Shull, M. Minerals, M.S. Meeting, T.C.o.A. Phases, CALPHAD and Alloy Thermodynamics: Proceedings of a Symposium Sponsored by

the Alloy Phase Committe of the Joint Structural Materials Division (SMD) and the Electronic, Magnetic & Photonic Materials Division (EMPMD) of TMS (The Minerals, Metals & Materials Society), Held During the 2002 TMS Annual Meeting in Seattle, Washington, February 17-21, 2002, to Honor of the William Hume-Rothery Award Recipient, Dr. Larry Kaufman, TMS (The Minerals, Metals & Materials Society)2002.

[29] D. Kim, B.-J. Lee, N.J. Kim, Thermodynamic approach for predicting the glass forming ability of amorphous alloys, Intermetallics 12 (2004) 1103-1107.

[30] D. Kim, B.-J. Lee, N.J. Kim, Prediction of composition dependency of glass forming ability of Mg–Cu–Y alloys by thermodynamic approach, Scripta Mater. 52 (2005) 969-972.

[31] H. Bo, J. Wang, S. Jin, H.Y. Qi, X.L. Yuan, L.B. Liu, Z.P. Jin, Thermodynamic analysis of the Al–Cu–Zr bulk metallic glass system, Intermetallics 18 (2010) 2322-2327.

[32] N. Saunders, A.P. Miodownik, CALPHAD: a Compre-hensive Guide Elsevier Science, New York (1998).

[33] A.T. Dinsdale, Sgte Data for Pure Elements, Calphad 15 (1991) 317-425.

[34] N. Saunders: Fe-Data Thermodynamic Database. [3.0], ThermoTech Ltd., Guildford, United Kingdom, 2001.

[35] Scientific Group Thermodata Europe, http://www.sgte.org/ (2008).

[36] Z.P. Lu, C.T. Liu, Glass formation criterion for various glass-forming systems, Phys. Rev. Lett. 91 (2003) 115505.

[37] Y. Waseda, H.-S. Chen, K. Thomas Jacob, H. Shibata, On the glass forming ability of liquid alloys, Sci. Technol. Adv. Mater. 9 (2008) 023003.

[38] C.R. Cao, D.W. Ding, D.Q. Zhao, E. Axinte, H.Y. Bai, W.H. Wang, Correlation between glass transition temperature and melting temperature in metallic glasses, Mater. Des. 60 (2014) 576-579.

[39] O. Kubaschewski, Iron Binary Phase Diagrams, Springer, Berlin (1982).

[40] R. Haydock, R.L. Johannes, Electronic-Structure of Transition-Metal Laves Phases, J. Phys. F 5 (1975) 2055-2067.

[41] G. Schmid, Metal-Clusters and Cluster Metals, Polyhedron 7 (1988) 2321-2329.

[42] J.W. Lauher, Transition-Metal Clusters, Cluster Compounds and Bulk Metals -

Molecular-Orbital View, Abstr. Pap. Am. Chem. S 179 (1980) 124-INOR.

[43] O.A. Belyakova, Y.L. Slovokhotov, Structures of large transition metal clusters, Russ. Chem. B+ 52 (2003) 2299-2327.

[44] T.L. Wang, J.H. Li, B.X. Liu, Proposed thermodynamic method to predict the glass formation of the ternary transition metal systems, Phys. Chem. Chem. Phys. 11 (2009) 2371-2373.

[45] S.F. Guo, J.L. Qiu, P. Yu, S.H. Xie, W. Chen, Fe-based bulk metallic glasses: Brittle or ductile?, Appl. Phys. Lett. 105 (2014) 161901.

[46] H.S. Chen, H.J. Leamy, C.E. Miller, Preparation of Glassy Metals, Annu. Rev. Mater. Sci. 10 (1980) 363-391.

[47] J. Cheney, K. Vecchio, Evaluation of glass-forming ability in metals using multi-model techniques, J. Alloy. Compd. 471 (2009) 222-240.

[48] H. Teichler, Structural dynamics on the μs scale in molecular-dynamics simulated, deeply undercooled, glass-forming Ni0.5Zr0.5, J. Non-Cryst. Solids 293 (2001) 339-344.

[49] F. Faupel, P.W. Huppe, K. Ratzke, Pressure-Dependence and Isotope Effect of Self-Diffusion in a Metallic-Glass, Phys. Rev. Lett. 65 (1990) 1219-1222.

[50] X.P. Tang, U. Geyer, R. Busch, W.L. Johnson, Y. Wu, Diffusion mechanisms in metallic supercooled liquids and glasses, Nature 402 (1999) 160-162.

[51] J. Han, C. Wang, X. Liu, Y. Wang, Z.-K. Liu, J. Jiang, Atomic-Level Mechanisms of Nucleation of Pure Liquid Metals during Rapid Cooling, ChemPhysChem 16 (2015) 3916-3927.

[52] C. Guo, P.M. Kelly, Boron solubility in Fe–Cr–B cast irons, Mater. Sci. Eng. A 352 (2003) 40-45.

[53] T.B. Cameron, J.E. Morral, The solubility of boron in iron, MTA 17 (1986) 1481-1483.

[54] A. Malins, J. Eggers, C.P. Royall, S.R. Williams, H. Tanaka, Identification of long-lived clusters and their link to slow dynamics in a model glass former, J. Chem. Phys. 138 (2013) 12A535.

[55] E. Matsubara, S. Sato, M. Imafuku, T. Nakamura, H. Koshiba, A. Inoue, Y. Waseda, Structural study of Amorphous Fe70M10B20 (M=Zr, Nb and Cr) alloys by X-ray

diffraction, Mater. Sci. Eng. A 312 (2001) 136-144.

[56] A.L. Greer, Metallic glasses ... on the threshold, Mater. Today 12 (2009) 14-22.

[57] G. Krauss, Steels: Processing, Structure, And Performance ASM International (2005).

[58] J. Pan, Q. Chen, N. Li, L. Liu, Formation of centimeter Fe-based bulk metallic glasses in low vacuum environment, J. Alloy. Compd. 463 (2008) 246-249.

[59] J. Shen, Q.J. Chen, J.F. Sun, H.B. Fan, G. Wang, Exceptionally high glass-forming ability of an FeCoCrMoCBY alloy, Appl. Phys. Lett. 86 (2005) 151907.

Captions

Table 1 Formula unit and effects on amorphization of main potential phases near the eutectic point of Fe-based alloys. The dominant elements in each phase are identified by bold italic letters. Symbol ● denotes positive; × denotes negative.

Table 2 Alloy compositions for experiment and the reactions upon cooling calculated from phase diagram.

Table 3 Effect of various elements on the main potential phases (● positive; ○ moderate; × negative).

Table 4 Typical systems of Fe-based BMGs [2].

Fig. 1. Structural stabilities of the crystalline clusters of various pure metals with coordination numbers of 12-14: red represents stable or metastable and blue represents unstable [51].

Fig. 2. Temperature dependence of mole fraction of Fe, Cr and C in each phase.

Fig. 3. XRD patterns of various Fe-based alloys during rapid cooling.

Fig. 4. Flow diagram of composition design protocol for BMGs.

Fig. 5. Calculated isopleth section of $Fe_{63-x}Cr_{16}Mo_{13}B_6Y_2C_x$ multi-component phase diagram. The grey area represents the region of easy glass-forming according to the phase selection principle. The dotted lines denote two compositions inside and outside the grey area for experiments.

Fig. 6. Temperature dependence of mass fraction of phases for (a) $Fe_{53}Cr_{16}Mo_{13}B_6Y_2C_{10}$ and (b) $Fe_{50}Cr_{16}Mo_{13}B_6Y_2C_{13}$ alloys.

Fig. 7. XRD patterns and EPMA of as-cast (a) $Fe_{53}Cr_{16}Mo_{13}B_6Y_2C_{10}$ and (b) $Fe_{50}Cr_{16}Mo_{13}B_6Y_2C_{13}$ rods with a diameter of 3 mm.

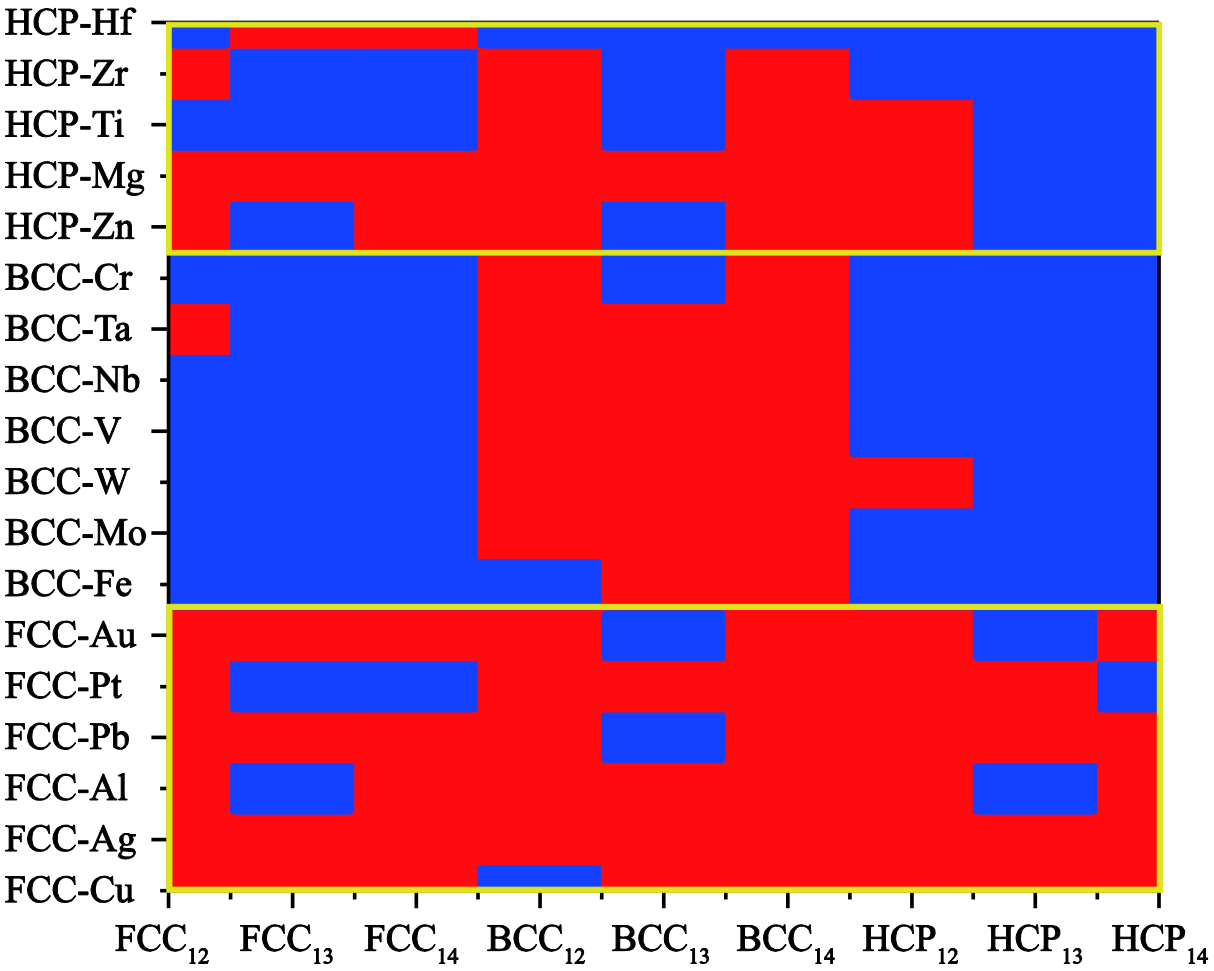

Fig. 1. Structural stabilities of the crystalline clusters of various pure metals with coordination numbers of 12-14: red represents stable or metastable and blue represents unstable [51].

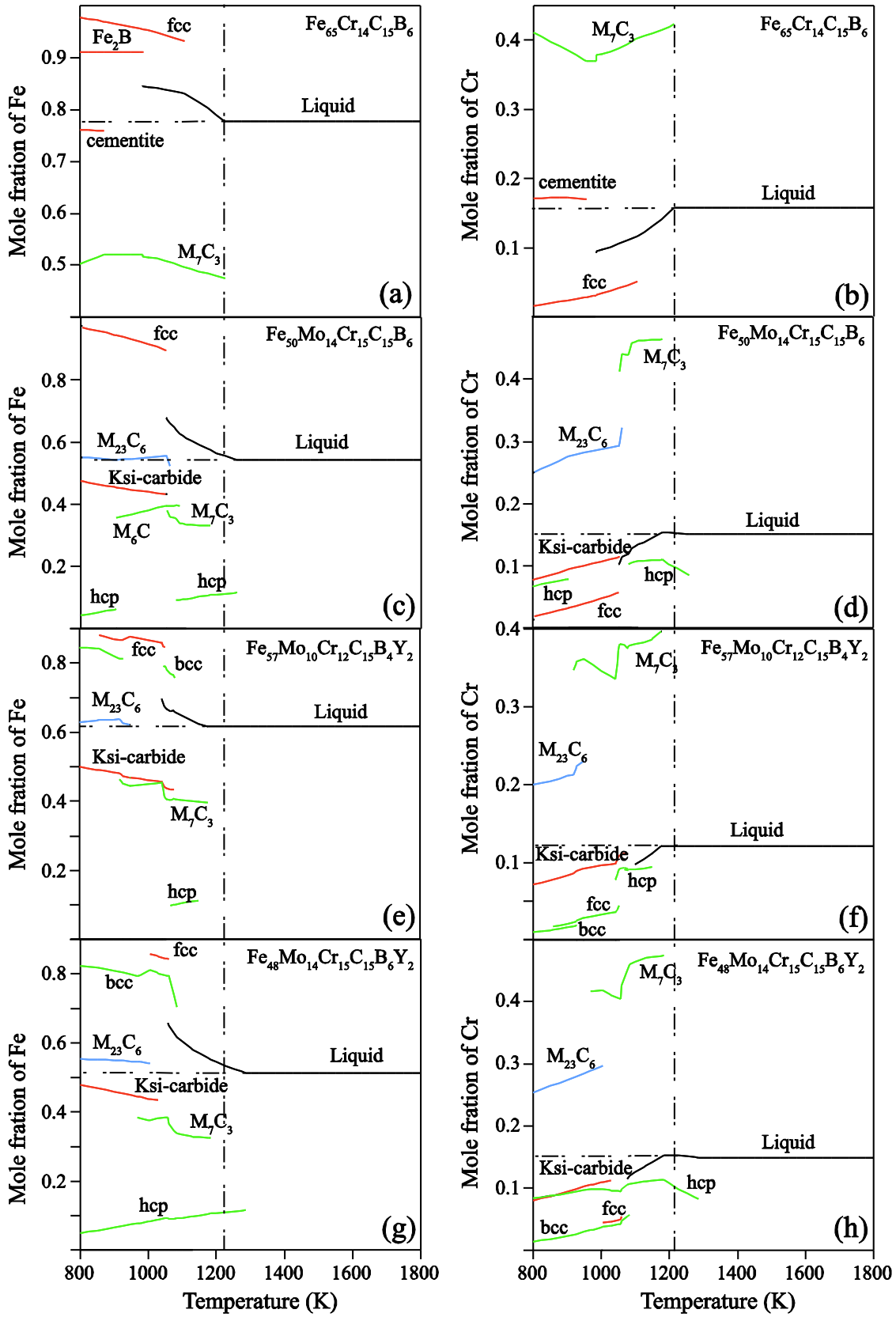

Fig. 2. Temperature dependence of mole fraction of Fe, Cr and C in each phase.

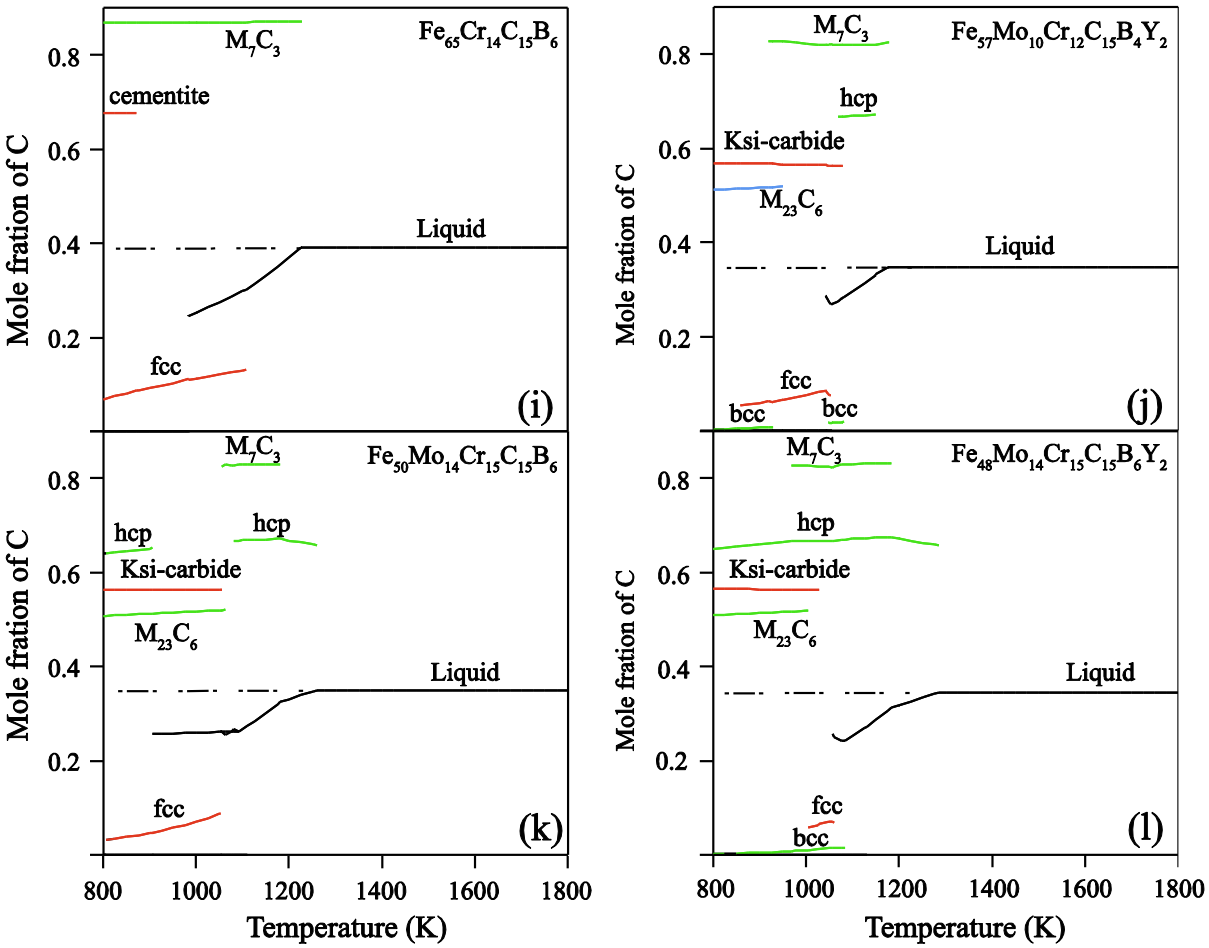

Fig. 2. (continue)

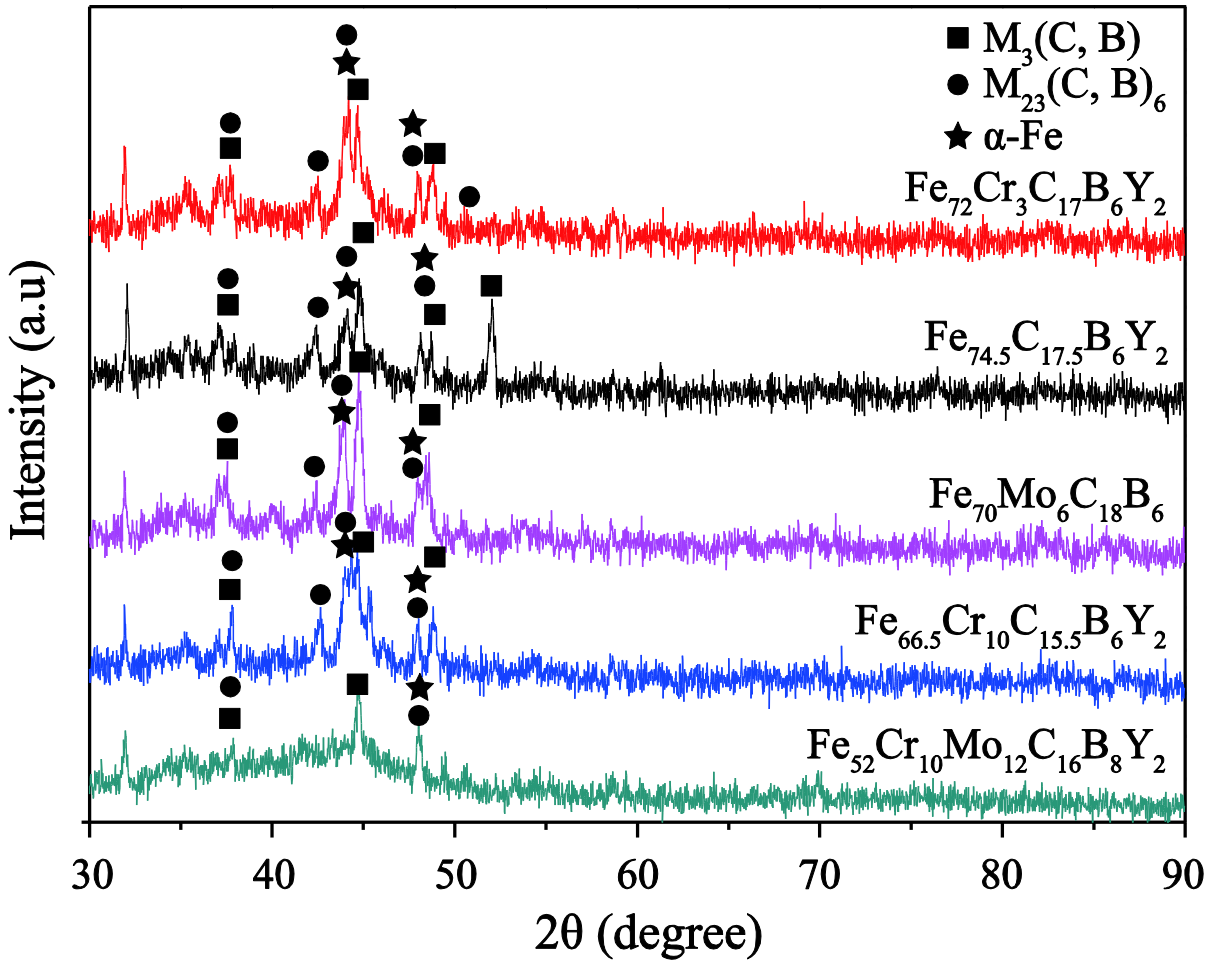

Fig. 3. XRD patterns of various Fe-based alloys under the condition of rapid cooling.

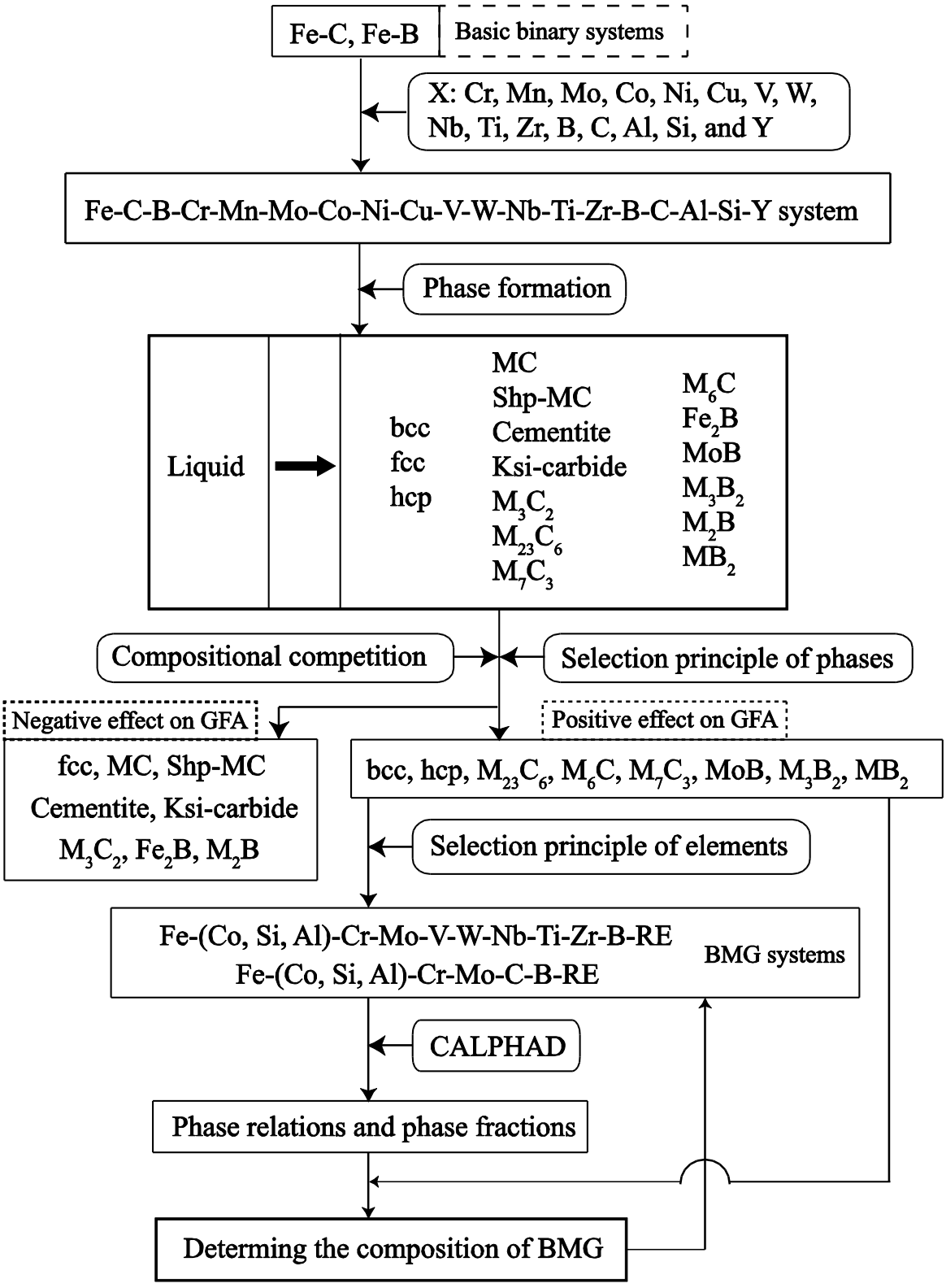

Fig. 4. A flow diagram of composition design protocol for BMGs.

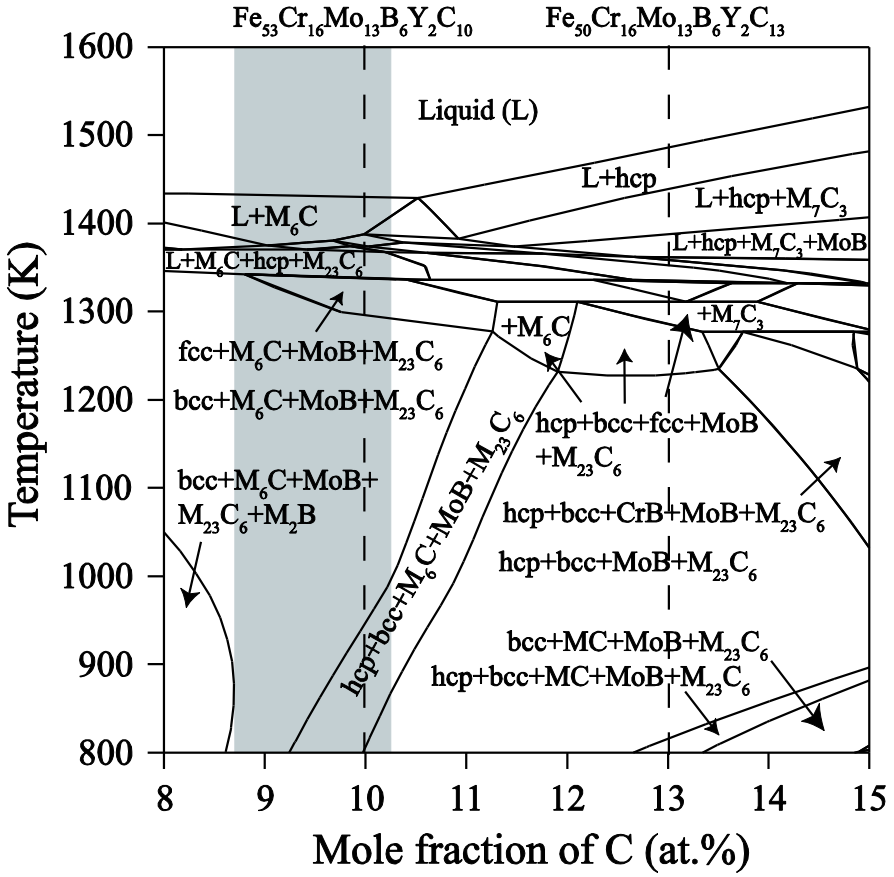

Fig. 5. Calculated isopleth section of phase $Fe_{63-x}Cr_{16}Mo_{13}B_6Y_2C_x$ multi-component phase diagram. The grey area represents the region of easy glass-forming according to the phase selection principle. The dotted lines denote two compositions inside and outside the grey area for experiments.

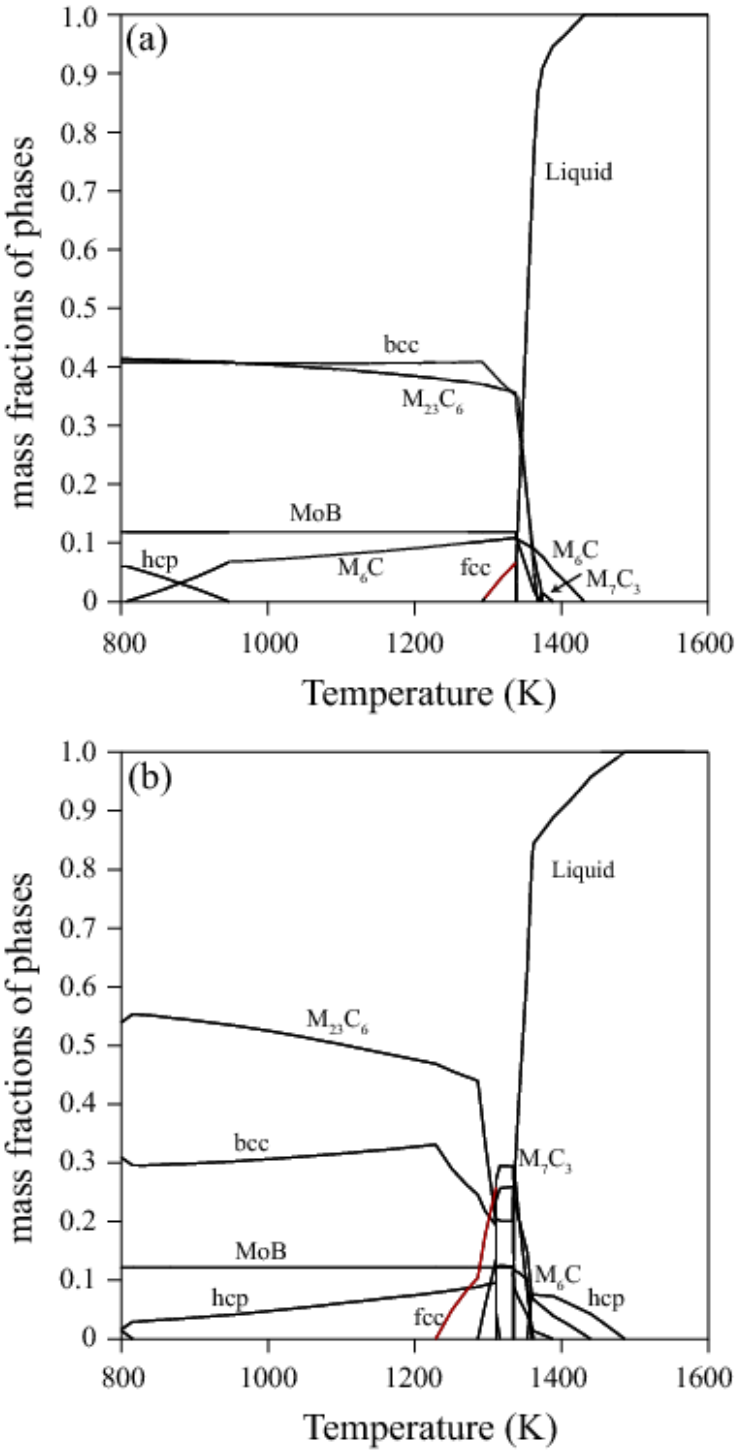

Fig. 6. Temperature dependence of mass fraction of phases for (a) $Fe_{53}Cr_{16}Mo_{13}B_6Y_2C_{10}$ and (b) $Fe_{50}Cr_{16}Mo_{13}B_6Y_2C_{13}$ alloys.

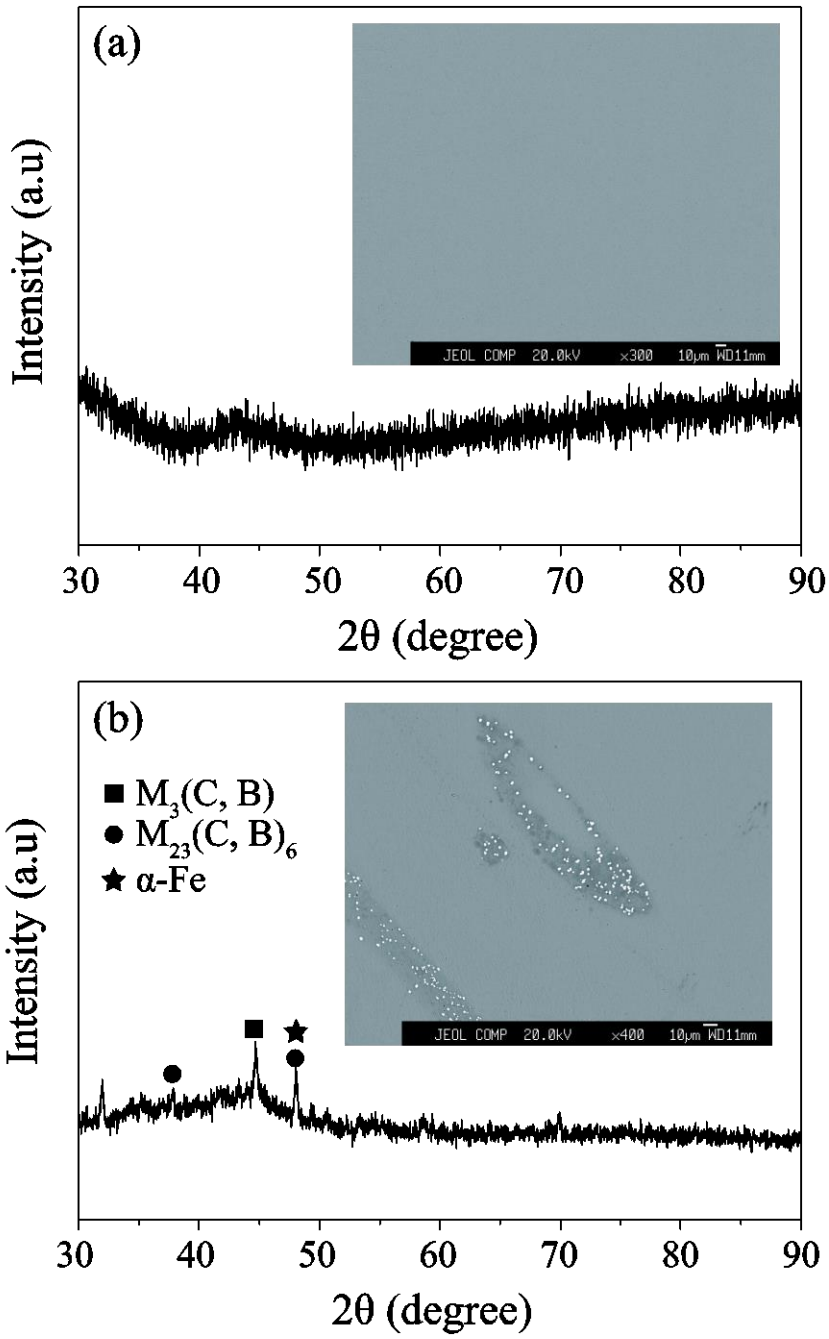

Fig. 7. XRD patterns and EPMA of as-cast (a) $Fe_{53}Cr_{16}Mo_{13}B_6Y_2C_{10}$ and (b) $Fe_{50}Cr_{16}Mo_{13}B_6Y_2C_{13}$ rods with a diameter of 3 mm.

Table 1 Formula unit and effects on amorphization of main potential phases near the eutectic point of Fe-based alloys. The dominant elements in each phase are identified by bold italic letters. Symbol ● denotes positive; × denotes negative.

Phase	formula unit	effect
bcc	(Al, B, Co, ***Cr***, Cu, ***Fe***, Mn, ***Mo***, ***Nb***, Ni, Si, ***Ti***, ***V***, ***W***, Y, Zr)$_1$(B, C, ***Va***)$_3$	●
hcp	(Al, B, ***Co***, Cr, Cu, Fe, Mn, Mo, Nb, Ni, Si, ***Ti***, V, W, Y, ***Zr***, ...)$_1$(B, C, ***Va***)$_{0.5}$	●
fcc	(***Al***, B, ***Co***, Cr, ***Cu***, ***Fe***, Mn, Mo, Nb, ***Ni***, Si, Ti, V, W, Y, Zr)$_1$(B, C, ***Va***)$_1$	×
MC	(V, Ti, Nb, Zr)$_1$C$_1$	×
Shp-MC	(Mo, ***W***)$_1$C$_1$	×
Cementite	(Co, Cr, ***Fe***, Mn, Mo, Nb, Ni, V, W)$_3$C$_1$	×
Ksi-carbide	(Cr, Fe, ***Mo***, W)$_3$C$_1$	×
M_3C_2	(Cr, Fe, Mn, Mo, V, W)$_3$C$_2$	×
$M_{23}C_6$	(Co, ***Cr***, ***Fe***, Mn, Ni, V)$_{20}$(Co, ***Cr***, ***Fe***, Mn, ***Mo***, Ni, V, W)$_3$C$_6$	●*
M_6C	(Co, Fe, Ni)$_2$(Mo, ***W***)$_2$(Co, Fe, Ni, ***Mo***, ***W***)$_2$C$_1$	●
M_7C_3	(Co, ***Cr***, Fe, Mn, Mo, Ni, V, W)$_7$C$_3$	●
Fe_2B	Fe_2B	×
MoB	$Mo_{0.5}B_{0.5}$	●
M_3B_2	(Cr, Fe, Mo, Ni, W)$_{0.4}$(Cr, Fe, Ni)$_{0.2}$B$_{0.4}$	●
M_2B	(Cr, Fe, Mo, Ni, W)$_{0.667}$B$_{0.333}$	×
MB_2	(Ti, Al)$_1$B$_2$	●
Graphite	B, ***C***	×

*only without the formation of austenite

Table 2 Alloy compositions for experiment and the reactions upon cooling calculated from phase diagram.

System	Reactions
$Fe_{72}Cr_3C_{17}B_6Y_2$	cementite→cementite+fcc→cementite+Fe_2B+bcc+fcc
$Fe_{74.5}C_{17.5}B_6Y_2$	cementite→cementite+fcc→cementite+Fe_2B+bcc+fcc
$Fe_{70}Mo_6C_{18}B_6$	cementite→cementite+fcc→cementite+fcc+MoB
$Fe_{66.5}Cr_{10}C_{15.5}B_6Y_2$	M_7C_3→fcc+M_7C_3→cementite+fcc+M_7C_3
$Fe_{52}Cr_{10}Mo_{12}C_{16}B_8Y_2$	hcp→hcp+MoB→hcp+MoB+M_7C_3

Table 3 Effect of various elements on the main potential phases (● positive; ○ moderate; × negative).

	bcc (ferrite)	hcp	fcc (austenite)	cementite	carbide	$M_{23}C_6$	M_6C	M_7C_3	MC	M_aB_b	MB_2	GRAPHITE
Co	×	●	○	○	×	○	●	○	×	○	×	●
Ni	×	○	●	○	×	○	●	○	×	●	×	●
Mn	×	×	●	○	×	○	×	○	×	×	●	×
Cr	●	○	×	○	○	●	×	●	×	○	●	×
Mo	●	○	×	○	●	●	●	○	○	●	●	×
V	●	○	×	○	×	○	×	○	●	●	●	×
W	●	○	×	○	○	○	●	○	○	●	×	×
Nb	○	○	×	○	×	×	×	×	●	×	●	×
Ti	●	●	×	×	×	×	×	×	●	×	●	×
Zr	○	●	×	×	×	×	×	×	●	×	●	×
Si	●	×	×	×	×	×	×	×	×	×	×	●
Cu	×	○	○	×	×	×	×	×	×	×	×	●
Al	●	○	×	×	×	×	×	×	×	×	×	○
Y	×		×						×			●

Table 4 Typical systems of Fe-based BMGs [2].

System	Alloy	Ref.
Fe-(Al, Ga)-(P, C, B, Si)	$Fe_{72}Al_{l5}Ga_2P_{11}C_6B_4$	95 Inoue
	$Fe_{72}Al_5Ga_2P_{11}C_5B_4Si_1$	95 Inoue
(Fe, Co, Ni)-(Zr, Nb, Ta, Hf, Mo, Ti, V, W)-B	$Fe_{70}Nb_{10}B_{20}$	01 Matsubara
	$(Fe_{0.75}B_{0.15}Si_{0.1})_{96}Nb_4$	03 Inoue
	$Fe_{60}Co_8Zr_{10}Mo_5W_2B_{15}$	01 Zhang
	$Fe_{63}Zr_8Co_6A_{l1}Mo_7B_{15}$	04 Lu
	$Fe_{45}Cr_{16}Mo_{16}C_{18}B_5$	01 Pang
	$(Fe_{44.3}Cr_{10}Mo_{12.8}Mn_{11.2}C_{15.8}B_{5.9})_{99.8}Y_{1.5}$	04 Lu
Fe-(Cr, Mn)-(Mo, Co)-(C, B)-(Er, Y)	$Fe_{56}Mn_5Cr_7Mo_{12}Er_2C_{12}B_6$	05 Luo
	$Fe_{63}Mo_{14}Er_2C_{15}B_6$	05 Luo
	$Fe_{48}Cr_{15}Mo_{14}Er_2C_{15}B_6$	04 Ponnambalam
	$Fe_{41}Co_7Cr_{15}Mo_{14}C_{15}B_6Y_2$	05 Shen

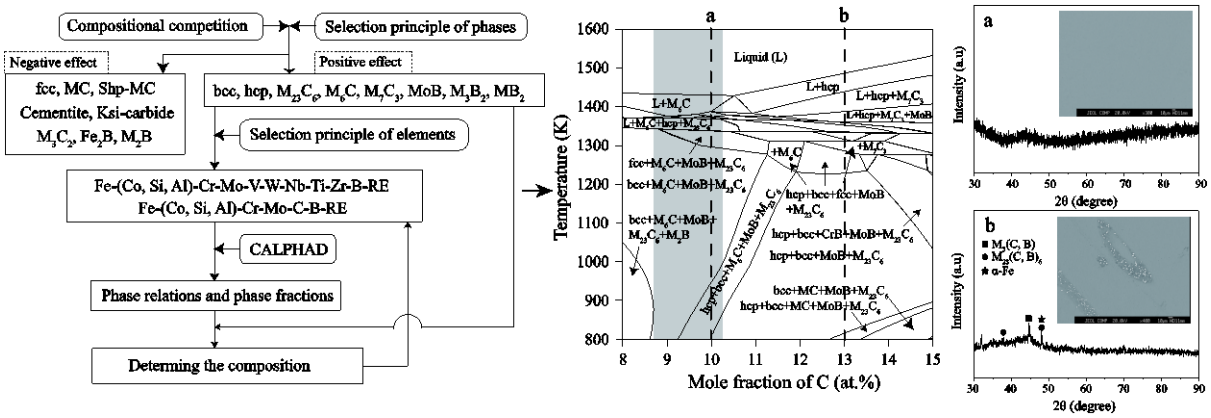

Graphical abstract

Highlights

- An accurate and effective composition design protocol for Fe-based multi-component bulk metallic glass was firstly proposed.
- The protocol emphasizes the process of nucleation in terms of compositional and structural fluctuations, other than the melting point that is focused before.
- Selection principles of phases and sixteen elements are tabulated and facilitate the composition design.